# Radiation Effects Due to 3 MeV Proton Irradiations on Back-Side Illuminated CMOS Image Sensors *

Xiang Zhang(张翔)[1,2,3], Yu-Dong Li(李豫东)[1,2], Lin Wen(文林)[1,2], Dong Zhou(周东)[1,2], Jie Feng(冯婕)[1,2], Lin-Dong Ma(马林东)[1,2,3], Tian-Hui Wang(王田珲)[1,2,3], Yu-Long Cai(蔡毓龙)[1,2,3], Zhi-Ming Wang(王志铭)[1,2,3], Qi Guo(郭旗)[1,2]**

[1]*Key Laboratory of Functional Materials and Devices for Special Environments, Xinjiang Technical Institute of Physics and Chemistry, Chinese Academy of Sciences, Urumqi 830011*

[2]*Xinjiang Key Laboratory of Electronic Information Materials and Devices, Urumqi 830011*

[3]*University of Chinese Academy of Sciences, Beijing 100049*

(Received 28 December 2017)

*Benefitting from the higher quantum efficiency and sensitivity compared with the front-side illumination (FSI) CMOS image sensors (CISs), backside illumination (BSI) CMOS image sensors tend to replace CCDs and FSI CISs for space applications. However, the radiation damage effects and mechanisms of BSI CISs in the radiation environment are not well understood. We provide radiation effects due to 3 MeV proton irradiations of BSI CISs dedicated to imaging by the analyses of mean dark current increase, dark current nonuniformity and full well capacity in pixel arrays and isolated photodiodes. Additionally, the present annealing certifies the radiation-induced defects, which are responsible for the parameter degradations in BSI CISs.*

*PACS:* 42.88.+h, 85.60.Dw, 05.40.−a DOI: 10.1088/0256-307X/35/7/074201

Backside illuminated (BSI) CMOS image sensors (CISs) are the result of the sustained developments in the image-dedicated CMOS technology. The performance of these devices exceeds that of conventional CISs based on 3 T pixels and front-side illumination (FSI) CISs, especially in the aspects for quantum efficiency and sensitivity. With the backside-thinned structure and converse illuminated direction, however, BSI CISs show differences on the radiation behavior. It is therefore necessary to study the radiation degradations of BSI CISs for scientific applications, particularly for space missions. BSI CISs have already been widely used for commercial applications and tend to be applied to space environments suffering harsh irradiation. Few researches aiming at radiation degradations of BSI CISs have been proposed previously.[1] Moreover, owing to the particular structure of BSI CISs (thinner back side and the unique back oxide layer as shown in Fig. 1),[2] radiation data obtained from FSI CISs previously may not be applied to BSI CIS devices directly.[3–5]

In this Letter, we report the results of radiation induced performance degradations, in two types of scientific BSI CISs with different epitaxial layer depths manufactured in 0.18 μm CMOS processes. Dark current and electro-optic performances are characterized before and after 3 MeV proton irradiations (up to a displacement damage dose (DDD) of $9.92 \times 10^8$ MeV/g) through the discrimination of ionizing effects and displacement damage effects. The analyses for mean dark current increase, dark current nonuniformity and full well capacity are accomplished since these parameters are susceptibility under the irradiation conditions and, meanwhile, are crucial to the quality of the acquired images.

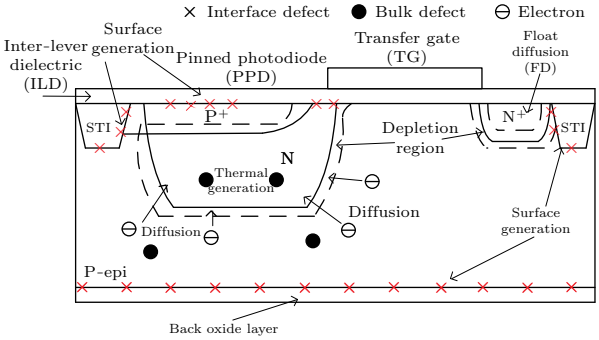


**Fig. 1.** Cross section of pixel structure in BSI CISs and the origins of dark current increase after irradiation.

The studied devices are one piece for TVISB with a thicker epi-layer around 10 μm and another for VIS with a thinner epi-layer around 3 μm. These two versions of BSI CISs are fabricated in similar structure except the thickness of the epi-layer as illustrated above, in which there are a thinner epi-layer and an additional back oxide layer compared with FSI CIS devices. Their pixel arrays are constituted by 2048 × 2048 pixels featuring 11 μm pitch with 4 T pixel CISs manufactured in 0.18 μm CMOS process dedicated to imaging. The photodiode structure makes use of the pinned photodiode. The isolation method is

*Supported by the National Natural Science Foundation of China under Grant No 11675259, the National Defense Pre-research Foundation of China under Grant No 6140A2404051, and the West Light Foundation of Chinese Academy of Sciences under Grant Nos 2016-QNXZ-B-8 and 2016-QNXZ-B-2.

**Corresponding author. Email: guoqi@ms.xjb.ac.cn

shallow trench isolation (STI). The pixel array works on the rolling shutter mode with correlated double sampling and features an extremely low temporal dark noise of $1.6e^-$. The peak QE can reach around 95%.

**Table 1.** Proton irradiation conditions are presented in the forms of fluences, TID and DDD.

| Fluences ($10^{10}$ p/cm$^2$) | TID (krad) | DDD ($10^8$ MeV/g) |
|---|---|---|
| 1.47 | 20 | 3.30 |
| 2.94 | 40 | 6.60 |
| 4.41 | 60 | 9.90 |

The pixel array was divided into four districts and exposed un-biased (as the same trend and neglectable difference among various bias states)[4] 3 MeV protons with fluences from 0 to $4.41 \times 10^{10}$ proton/cm$^2$ (as listed in Table 1). Aluminum degraders were used to cover the unirradiated districts. Afterwards, the devices have been annealed at room temperature, 100 °C and 150 °C. The irradiation facilities are $2 \times 6$ MeV EN tandem electrostatic accelerators at the Institute of Heavy Ion Physics, Peking University. The anneal experiments and CIS parameter test are implemented in the Xinjiang Technical Institute of Physics and Chemistry, Chinese Academy of Sciences. All irradiations and measurements were carried out at room temperature.

When the BSI CISs are irradiated by protons, the total ionizing dose (TID) and displacement damage (DD) have an impact on the generated defects simultaneously and result in several mechanisms contributing to the obtained dark current increase. These origins of additional dark current (as shown in Fig. 1) involve the following aspects: a surface leakage current (caused by interface states), a bulk diffusion current (originated from displacement defects in the bulk around the depletion region), and a depletion region leakage current (including the thermal generation current resulted from point defects and cluster defects in the depletion region).[6] Due to the thinner epi-layer, a back-side passivation layer exists to achieve surface modification and acts as a novel origin compared with FSI CISs.

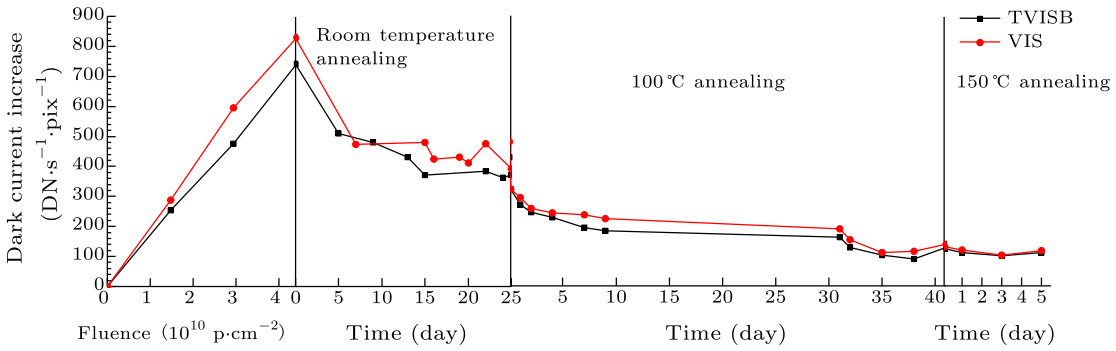


**Fig. 2.** Mean dark current increase related to the proton fluence and the annealing data at room temperature, 100 °C and 150 °C. A discrimination between the mean dark current increase of TVISB and VIS is presented. Eventually, the data gathered to a similar level.

The number of pixels in the pixel arrays, divided into four areas, is enough to obtain the statistical distribution of dark current increase. The results of dark current increase induced by proton irradiations and the following annealing outcomes as a function of fluences are presented in Fig. 2. Mean dark currents of the two device types both increase nearly linearly against the fluences of protons. Such a relationship is mainly subject to the defects in the depletion region, which act as classical Shockley–Read–Hall (SRH) generators.[7,8]

After irradiation, the devices underwent a series of annealing processes containing room temperature (about 23 °C) annealing for 25 days, 100 °C annealing for 41 days, and 150 °C annealing for 5 days. For TVISB (the similar trend for VIS during annealing), at the end of room temperature annealing, the mean dark current increase remained 50.1%. This dramatic reduction of dark current is aroused by the removal of oxide trapped charge during the room temperature annealing. Two mechanisms concerning oxide trapped charge are related to this decrease: (1) the local high electric field at the overlap of pinned photodiode (PPD) and transfer gate (TG) induced by oxide trapped charge prompt the Poole–Frenkel effect and phonon-assisted tunneling, as shown in Fig. 3(a);[9] (2) a positive electric field caused by the oxide trapped charge in shallow trench isolation (STI) formed an additional depletion region extending the edge of depletion region around the surface of oxide, as a result, leading to an extra surface leakage current contributing to the dark current increase, as shown in Fig. 3(b). Along with the annealing of oxide trapped charge, these influences gradually disappeared. When the 25-day 100 °C annealing finished, 17.3% dark current increase was left. This recovery hints at the anneal of most interface states. After this step, most of the effects induced by TID are eliminated, and a slight decrease for 2.1% following the 5-day 150 °C annealing was obtained, which stood for the anneal of P-V center. Then, the last 15.2% dark current increase is governed by the remaining displacement defects; they

play roles as generation centers and most of them are stable below 200 °C.[10]

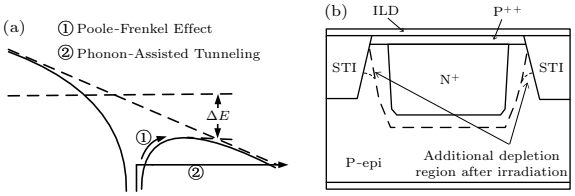


**Fig. 3.** Two mechanisms involving oxide trapped charge related to the decrease of mean dark current increase: (a) Poole–Frenkel effect and phonon-assisted tunneling, (b) depletion region extension close to the STI around PPD structure.

Figure 2 shows a discrimination of the dark current characteristics during proton irradiation between TVISB and VIS. We assume that this gap is caused by different epi-layer thicknesses, while Ref. [11] concluded that the impacts of radiation-induced degradation on FSI CISs contributed by different epi-layer thicknesses are negligible. These results correspond to a P-type substrate with high concentration doping under an epi-layer, which greatly reduces the contribution of charge from the backside passivation layer. With respect to BSI CISs, P-type substrate is cut down. Owing to the low doping concentration level of the epi-layer (several orders of magnitude lower compared with substrate), the diffusion length of minority carriers is strongly enhanced so that charge generation originated from interface states located on the back-oxide layer makes a significant contribution to the mean dark current increase. This reveals the source of the obtained discrimination in Fig. 2 since the epi-layer thicknesses for TVISB and VIS are respectively 10 μm and 3 μm and the thinner epi-layer means the shorter distance between the back-oxide layer and the depletion region. This is also evidenced by that, at the terminal of 150 °C annealing, both mean dark current increases of TVISB and VIS gathered to a similar level when the TID effect caused by proton irradiation almost disappeared.

In the following we investigate the dark current distributions of TVISB after proton irradiations and each anneal process, as presented in Figs. 4(a) and 4(b) separately. The pre-irradiation dark current distribution corresponds to a Gaussian. With the increase of proton fluence, two types of behavior were obtained in the semi-logarithmic scale: (1) the mean value of the Gaussian part moved to a higher level and the standard deviation also enhanced (the expansion of Gaussian shape), (2) and the form of hot pixel tail developed to a higher current value keeping its exponential behavior.[12,13]

The first effect is caused by TID and the elastic nuclear Coulombic scattering. The proton-induced TID effect achieves the creation of interface states in oxides acting as generation centers in the band gap and this establishment of defects influences all pixels in the CISs array. Concerning the displacement damage induced by the elastic nuclear Coulombic scattering, the cross section of this part is also important and the generated bulk defects have impacts on all of the irradiated pixels.[7] For these consequences above, the mean value of the Gaussian part obtained in Fig. 4(a) was enhanced against the proton fluence. This Gaussian part of the ultimate result after 150 °C anneal in Fig. 4(b), however, does not recover the initial shape. This remainder can be deduced as the expression of the displacement defects formed by the elastic nuclear Coulombic scattering.

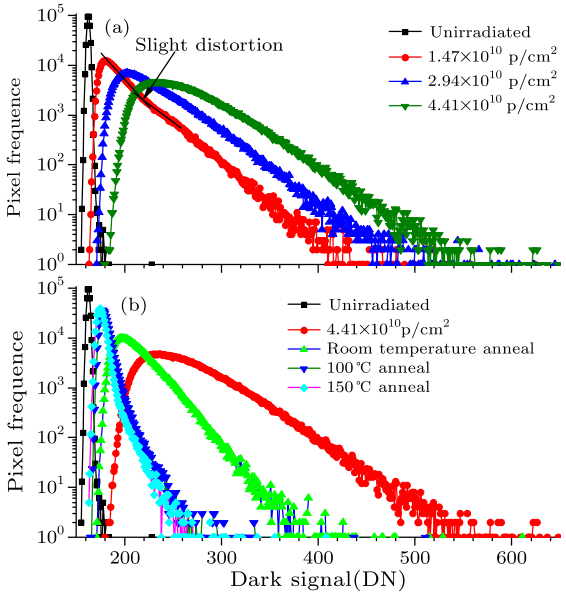


**Fig. 4.** Dark current distribution non-uniformity in the semi-logarithmic scale during (a) irradiation processes and (b) annealing processes.

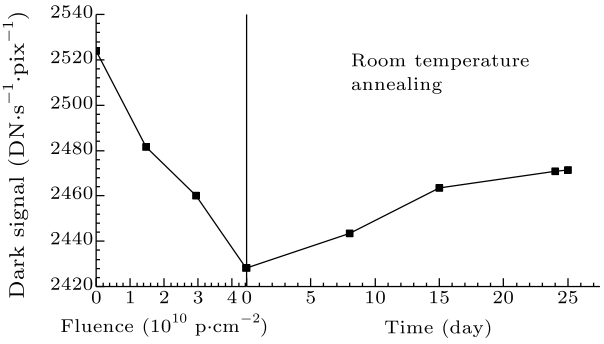


**Fig. 5.** Saturation output signal variation with the increase of fluences and during room temperature annealing.

For the second effect, the hot pixel tail presented in an exponential shape originated from the scarce nuclear collisions (including inelastic interaction nuclear reaction and elastic interaction nuclear force scattering) in the depleted region of pixels where the so-induced displacement defects act as generation centers. The cross sections of these collisions are extremely small so that the degradation caused by these mechanisms is independently varying from different

pixels. A slight distortion for the overlap of Gaussian and hot pixel tail is presented at the fluences of $1.47 \times 10^{10}\,\mathrm{p/cm^2}$, as presented in Fig. 4(a). With the increase of fluence, this distortion was covered by the superposition of numerous interactions and the expansion of the Gaussian. After 150 °C annealing, this distortion became obvious again with the shrinking of the Gaussian, as shown in Fig. 4(b).

Full well capacity (FWC), as a crucial parameter related to dynamic range, signal-to-noise ratio, etc., is discussed. FWC characterizes the maximum capacity in the potential well of PPD. The results of the TVISB FWC during irradiation and after room temperature annealing are shown in Fig. 5.

FWC can be simply expressed as

$$\mathrm{FWC} = (V_{\mathrm{pin}} - V_{\mathrm{TG-PD}}) \times C_{\mathrm{PPD}}, \qquad (1)$$

where $V_{\mathrm{pin}}$ is the highest potential in the buried n-well when TG is on, $V_{\mathrm{TG-PD}}$ is the lowest potential in the overlap of TG-PD when TG is off, and $C_{\mathrm{PPD}}$ is the equivalent capacitance of the depletion region between $V_{\mathrm{pin}}$ and $V_{\mathrm{TG-PD}}$ when TG is off. Thanks to the PPD structure, the $P^+$ layer acts as the isolation between the inter-level dielectric (ILD) and the depletion region so that the defects in ILD induced by TID do not make a significant influence on the parameter degradation. In other words, $V_{\mathrm{pin}}$ and $C_{\mathrm{PPD}}$ have slight changes during irradiation. However, concerning the STI close to TG, the oxide trapped positive charges bend down the energy level close to the interface of Si–$SiO_2$. This effect lowers the potential (for electrons) under TG (namely an increase on $V_{\mathrm{TG-PD}}$). Eventually, a reduction of FWC was presented. The mechanism described above is shown in Fig. 6.

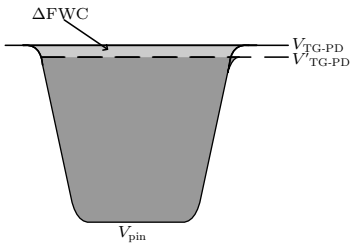


**Fig. 6.** The influence on the decrease of full well capacity induced by $V_{\mathrm{TG-PD}}$ reduction.

In summary, this work dedicates to the study of degradation mechanisms of BSI CISs after 3 MeV proton irradiation up to a DDD of $9.92 \times 10^8\,\mathrm{MeV/g}$. The mean dark current increases with DDD. Several mechanisms are involved including the Poole–Frenkel effect in the high electric field, phonon-assisted tunneling, depletion region extending and displacement defects in the depletion region leading to a classical SHR generation mechanism. According to the appearance during proton irradiation and annealing process, the back-oxide layer acts as a novel origin of mean dark current increase deduced from the comparison of TVISB and VIS. A conclusion can be made that the back-oxide-layer-induced contribution to the dark current degradation during proton irradiation cannot be ignored. Moreover, after proton irradiation, the dark current distribution is discussed. The Gaussian part moved to a higher level with width extending. These are caused by TID and the elastic nuclear Coulombic scattering. Additionally, a hot pixel tail appears on the dark current distribution and appears exponential. This phenomenon is induced by inelastic interaction nuclear reaction and elastic interaction nuclear force scattering. Finally, we present the degradation of the FWC in BSI CISs and describe its potential variation before and after the proton irradiation. A conclusion has been drawn that the oxide trapped positive charges in STI take charge of this degradation. We will carry out further research in the next step about radiation effects on BSI CISs induced by different particle types.

## References

[1] BenMoussa A, Gissot S F, Giordanengo B, Meynants, Xiongfei W, Wolfs B, Bogaerts J, Schuhle U, Berger G, Gottwald A, Laubis C, Korth Udo, Scholze F, Ali S and Saito T 2013 *IEEE Trans. Nucl. Sci.* **60** 3907
[2] Padmakumar R R, Christian L and Nihtianov S 2014 *IEEE Sens J.* 1660
[3] Wang B, Li Y D, Guo Q, Liu C J, Wen L, Ren D Y, Zeng J Z and Ma L Y 2015 *Acta Phys. Sin.* **64** 84209 (in Chinese)
[4] Wang F, Li Y D, Guo Q, Wang B, Zhang X Y, Wen L and He C F 2016 *Acta Phys. Sin.* **65** 024212 (in Chinese)
[5] Ma L D, Li Y D, Guo Q, Wen L, Zhou D, Feng J, Liu Y, Zeng J Z, Zhang X and Wang T H 2017 *Chin. Phys.* B **26** 114212
[6] Tan J M 2013 *PhD Dissertation* (Delft: Technische Universiteit Delft)
[7] Goiffon V, Virmontois C, Magnan P, Cervantes P, Corbiere F, Estribeau M and Pinel P 2010 *Proc. SPIE* **7826** 78261S
[8] Srour J R and Palko J W 2013 *IEEE Trans. Nucl. Sci.* **60** 1740
[9] Srour J R and Hartmann R A 1989 *IEEE Trans. Nucl. Sci.* **36** 1825
[10] Srour J R, Marshall C J and Marshall P W 2003 *IEEE Trans. Nucl. Sci.* **50** 653
[11] Virmontois C, Durnez C, Estribeau M, Cervantes P, Avon B, Goiffon V, Magnan P, Materne A and Bardoux A 2016 *IEEE Trans. Nucl. Sci.* **64** 38
[12] Beaumel M, Herve D and Aken D V 2010 *IEEE Trans. Nucl. Sci.* **57** 2056
[13] Virmontois C, Goiffon V, Magnan P, Girard S, Saint-Pe O, Petit S, Roll G and Bardoux A 2012 *IEEE Trans. Nucl. Sci.* **59** 927